

Online-updated High-order Collaborative Networks for Single Image Deraining

Cong Wang¹, Jinshan Pan², Xiao-Ming Wu^{1*}

¹ Department of Computing, The Hong Kong Polytechnic University

² School of Computer Science and Engineering, Nanjing University of Science and Technology
supercong94@gmail.com, sdluran@gmail.com, xiao-ming.wu@polyu.edu.hk

Abstract

Single image deraining is an important and challenging task for some downstream artificial intelligence applications such as video surveillance and self-driving systems. Most of the existing deep-learning-based methods constrain the network to generate derained images but few of them explore features from intermediate layers, different levels, and different modules which are beneficial for rain streaks removal. In this paper, we propose a high-order collaborative network with multi-scale compact constraints and a bidirectional scale-content similarity mining module to exploit features from deep networks externally and internally for rain streaks removal. Externally, we design a deraining framework with three sub-networks trained in a collaborative manner, where the bottom network transmits intermediate features to the middle network which also receives shallower rainy features from the top network and sends back features to the bottom network. Internally, we enforce multi-scale compact constraints on the intermediate layers of deep networks to learn useful features via a Laplacian pyramid. Further, we develop a bidirectional scale-content similarity mining module to explore features at different scales in a down-to-up and up-to-down manner. To improve the model performance on real-world images, we propose an online-update learning approach, which uses real-world rainy images to fine-tune the network and update the deraining results in a self-supervised manner. Extensive experiments demonstrate that our proposed method performs favorably against eleven state-of-the-art methods on five public synthetic datasets and one real-world dataset. The source code will be available at <https://supercong94.wixsite.com/supercong94>.

Introduction

Outdoor images taken in rainy conditions have limited visibility, which degrades the performance of various applications such as video surveillance and self-driving systems. Hence, it is essential to recover the degraded images to improve scene visibility and the performance of downstream applications. This paper considers single image deraining.

A rainy image O can be modeled as a linear combination of a rain-free image B and a rain streaks image R :

$$O = B + R. \quad (1)$$

*Corresponding author

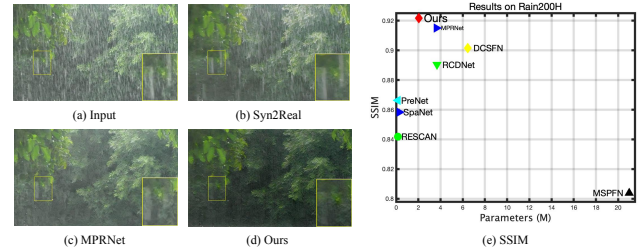


Figure 1: Results on the real-world image (b-d) and the synthetic Rain200H dataset (e). Our proposed method generates a better deraining result on the real-world image and achieves the best performance-parameter trade-off on the synthetic dataset.

Many deraining approaches have been developed based on this simple rainy image model, including prior-based methods and deep-learning-based methods. Prior-based methods usually explore empirical statistical properties of rain streaks and rain-free images, such as image decomposition (Kang, Lin, and Fu 2012), sparse coding (Luo, Xu, and Ji 2015; Zhang and Patel 2017), low-rank representation (Chen and Hsu 2013), and Gaussian mixture model (Li et al. 2016). However, since the priors are based on empirical statistical observations, they do not hold when real-world complex rainy conditions deviate from the simplified assumptions.

Recent years have witnessed the successful application of deep learning methods to image deraining (Fu et al. 2017; Yang et al. 2017; Li et al. 2018b; Zhang and Patel 2018; Pan et al. 2018; Wang et al. 2019a; Jiang et al. 2020; Wang et al. 2020b; Zamir et al. 2021; Wang et al. 2021; Pan et al. 2021). Most of these methods develop joint learning networks (Zhang and Patel 2018; Hu et al. 2019; Jiang et al. 2020) or explore multi-scale architectures (Wang et al. 2020b; Zhu et al. 2020; Zamir et al. 2021) for image deraining. The methods based on joint learning networks include density-guided multi-stream networks (Zhang and Patel 2018) and progressive networks motivated by patch similarity and guided by multi-scale architectures (Jiang et al. 2020). While these methods are able to remove rain streaks with the guiding networks, they do not perform well when the guiding process is not accurately estimated. In addition,

although multi-scale architectures have been demonstrated to be effective, existing methods usually adopt a straightforward way to fuse features from different scales and do not explore the properties of multi-scale features. Last but not least, existing methods commonly use synthetic datasets to train the deep models due to the lack of well-constructed real-world datasets. However, the gap between synthetic and real data limits the performance of these methods in real-world applications.

Due to the difficulty of single image deraining, how to fully utilize convolutional features from both shallow and deep layers of a deep model and explore multi-scale features are important for rain streaks removal. In addition, it is essential to develop an effective algorithm to improve the deraining performance on real-world images.

To this end, we propose a high-order collaborative network with multi-scale compact constraints and a bidirectional scale-content mining module to remove rain streaks. The high-order collaborative design allows exploring features from the shallower and deeper layers of different sub-networks collaboratively, while the multi-scale compact constraints are used to effectively learn features from intermediate convolutional layers and the bidirectional scale-content mining module is embedded in an encoder-decoder network to explore features of different scales.

Specifically, the high-order collaborative design contains three sub-networks (bottom, middle, and up) which are learned in a collaborative manner, where the bottom network transmits intermediate features to the middle network which also receives shallower rainy features from the top network and sends back features to the bottom network. The middle and top networks provide deep supervision for the bottom network to better learn and transmit shallow rainy features to higher layers to facilitate deraining. To generate more useful features from a deep network internally, we propose to enforce multi-scale compact constraints on the intermediate layers to learn better features with Laplacian pyramid images. In addition, we develop a bidirectional scale-content similarity mining module in a down-to-up and up-to-down manner to capture long-range dependencies between features at different scales, which is embedded in an encoder-decoder architecture to explore useful features.

Finally, to improve the model performance on real-world images, we propose a simple yet effective online-update learning approach, to fine-tune the model trained on synthetic datasets using real-world data in a self-supervised manner with a KL-Divergence loss function. The proposed network design and online-update learning approach enable our model to achieve state-of-the-art deraining performance, especially on real-world images, as illustrated in Fig. 1.

The main contributions of this paper include:

- We propose a collaborative deraining framework with multi-scale compact constraints to control the learning process in an external and internal manner, with a new bidirectional scale-content similarity mining module to adaptively learn richer feature representations.
- We present a simple yet effective online-update learning approach to fine-tune the model trained on syn-

thetic datasets to adapt to real rainy conditions in a self-supervised manner for real-world image deraining.

- We conduct extensive experiments and ablation studies to evaluate the proposed method. The results demonstrate that our method performs favorably against state-of-the-art methods with fewer parameters on both synthetic and real-world datasets.

Related Work

In this section, we briefly review recent works on image deraining, which are based on deep learning, as well as some image restoration methods based on similarity mining.

Single Image Deraining

In recent years, deep-learning-based approaches have dominated the research of image deraining due to the strong representation learning ability of deep neural networks. Fu et al. (2017) observe that high-frequency details provide more rain streaks details and less background interference and design a deep detail residual network to learn rain streaks. Some deraining methods explore the properties of multi-scale images. Wang et al. (2020b) propose a cross-scale framework to fuse features of different scales from sub-networks. Jiang et al. (2020) design a multi-scale progressive fusion network to transmit and fuse small-scale features to the original scale based on the similarity of multi-scale images. Recurrent networks are also used for deraining. Li et al. (2018b) develop a recurrent squeeze-and-excitation network with dilation convolution to model channel context relation. Ren et al. (2019) propose a progressive recurrent network to remove rain streaks stage by stage and analyze the effect of inputs, outputs, and loss functions for image deraining. Some non-local methods are based on attention mechanisms. Li et al. (2018a) propose to embed a non-local module to an encoder-decoder framework to capture long-range feature dependency for improving representation learning. Wang et al. (2020a) attempt to combine self-attention and scale-aggregation in a self-calibrated network. Besides, some semi-supervised approaches have been proposed for removing rain streaks in real-world images. For example, Wei et al. (2019) develop a semi-supervised transfer learning approach, and Yasarla, Sindagi, and Patel (2020) design a Gaussian-process-based model that learns on both synthetic and real data.

Different from the above works, our proposed method aims to explore inner structures and useful features of the deraining network in an external and internal manner to train the network for better rain streaks removal. We also propose an effective online-update learning approach to fine-tune the model trained with synthetic data on real data for real-world image deraining.

Similarity Mining

Similarity mining aims to find the most matched content at the feature level. Mei et al. (2020b) study cross-scale feature mining by exploring the inherent properties of images for single image super-resolution. Mei et al. (2020a) mine the

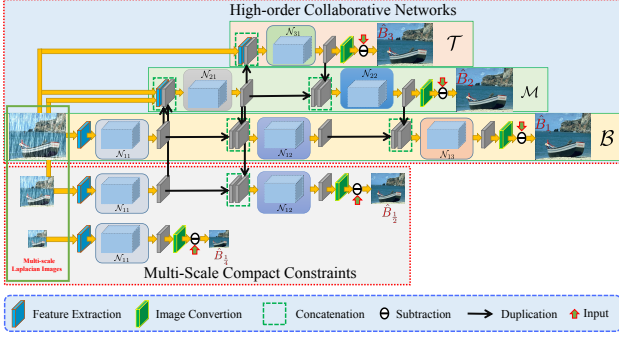


Figure 2: Proposed high-order collaborative networks with multi-scale compact constraints. Each network module \mathcal{N}_{mn} has a same encoder-decoder structure with the bidirectional scale-content similarity minding module shown in Fig. 3.

similarity from coarser to finer levels in a multi-scale manner for image restoration. Different from these works that only explore single directional mining (from coarser to finer levels), we in this paper design a bidirectional scale-content similarity mining module to adaptively learn richer features for better deraining.

Proposed Method

In this section, we introduce each element of the proposed method including high-order collaborative network, multi-scale compact constraint, encoder-decoder structure with a bidirectional scale-content similarity mining module, supervised loss function, and online-update learning.

High-order Collaborative Networks

How to exploit features from the intermediate layers and different modules in a collaborative manner is important for image restoration. Here, we design an effective high-order collaborative network¹ to assist each sub-network to learn features in an external manner for better image deraining. The overall network structure of the high-order collaborative network is shown in Fig. 2, which consists of three sub-networks with similar structure. The bottom (\mathcal{B}), middle (\mathcal{M}), and top (\mathcal{T}) sub-networks respectively contain three, two, and one encoder-decoder component with a bidirectional scale-content similarity mining module that will be explained in detail in Sec. .

The three sub-networks can transmit shallower and deeper rainy features to each other in a collaborative manner to improve the performance of the deraining network \mathcal{B} . Note that \mathcal{M} and \mathcal{T} are supervised by ground truth, which can be regarded as a sort of deep supervision in an external manner such that \mathcal{M} and \mathcal{T} can transmit useful features to assist \mathcal{B} to learn better features for deraining. The three sub-networks are trained by:

$$\mathcal{L}_{\text{collaborative}} = \sum_{i=1}^3 \alpha_i (-SSIM(\hat{B}_i, B)), \quad (2)$$

¹We regard two-stream networks as collaborative networks and three-stream networks as high-order.

where $\{\hat{B}_i\}$ ($i = 1, 2, 3$) denote the output of networks \mathcal{B} , \mathcal{M} , and \mathcal{T} respectively, B is the ground truth, and α_i are weight parameters.

Multi-Scale Compact Constraints

Although the high-order collaborative design enables the bottom sub-network \mathcal{B} to exploit deeper and shallower features from the other two sub-networks, the features of each intermediate convolutional layer are learned without any constraints, making the solution space too large.

To regularize the solution space of intermediate convolutional layers, we design multi-scale compact constraints (MSCC) in an internal manner to enforce the network modules \mathcal{N}_{11} , \mathcal{N}_{12} , and \mathcal{N}_{21} , which are parts of the sub-networks \mathcal{B} and \mathcal{M} , to learn more useful features to facilitate image deraining. The multi-scale compact constraints are motivated by the multi-scale Laplacian images which can better model image structures than the original scale image. We use them to constrain the intermediate convolutional layers of the network.

We first obtain the Laplacian pyramid images and then use the scaled images to constrain the modules \mathcal{N}_{11} , \mathcal{N}_{12} , \mathcal{N}_{21} as shown in Fig. 2. Specifically, the multi-scale compact constraints are enforced by:

$$\mathcal{L}_{\text{mscc}} = \sum_{j=1}^2 \beta_j (-SSIM(\hat{B}_{\frac{1}{2^j}}, B_{\frac{1}{2^j}})), \quad (3)$$

where $\hat{B}_{\frac{1}{2^j}}$ are the output of intermediate layers as denoted in Fig. 2, $B_{\frac{1}{2^j}}$ are the corresponding $\frac{1}{2^j}$ scale Laplacian pyramid rain-free images, and β_j are weight parameters.

Encoder and Decoder with BiSCSM

Further, we develop a bidirectional scale-content similarity mining module (BiSCSM) to explore similar features from different scales, which is motivated by Mei et al. (2020c,b). The architecture is shown in Fig. 3.

The proposed BiSCSM contains Down-to-Up mining and Up-to-Down mining modules. The Up-to-Down mining module is defines as:

$$y_{i,j}^{p \times p} = \frac{1}{\sigma(x,z)} \sum_{g,h} \phi(x_{i,j}^{p \times p}, z_{u,v}^{p \times p}) \theta(x_{g,h}^{p \times p}), \quad (4)$$

where $\phi(x_{i,j}^{p \times p}, z_{u,v}^{p \times p}) = e^{(W_f x_{i,j}^{p \times p})^T (W_g z_{u,v}^{p \times p})}$, $\theta = W_\theta x_{g,h}^{p \times p}$, $\sigma = \sum_{u,v} \phi(x_{i,j}^{p \times p}, z_{u,v}^{p \times p})$, $y_{i,j}^{p \times p}$ is a $p \times p$ feature patch located at (i, j) , and W_f, W_g, W_θ are learnable filters. The Down-to-Up mining module is defined similarly as shown in Fig. 4.

Our proposed BiSCSM is different from the one in Mei et al. (2020c,b) which only mines patch similarity in a single direction. Our Down-to-Up mining and Up-to-Down mining modules enable capturing bidirectional similar content from large to small scales and from small to large scales to mine rich rainy features. The BiSCSM is embedded in an encoder-decoder framework as in Fig. 3 to learn useful features for rain streaks removal. We also use positional embedding to encode relations among rain streak features. Finally, we fuse the learned features at difference scales.

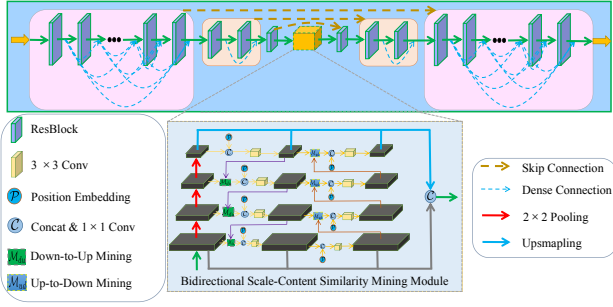


Figure 3: Proposed encoder and decoder with a bidirectional scale-content similarity mining module. The Down-to-Up and Up-to-Down mining modules are shown in Fig. 4.

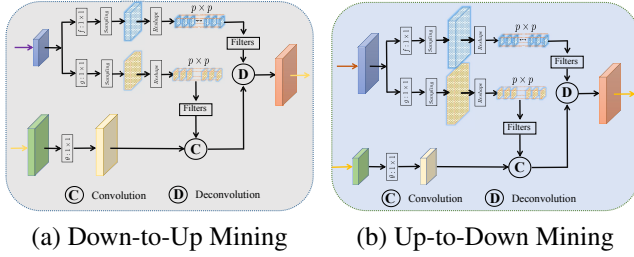


Figure 4: The scale-content similarity mining modules.

Supervised Loss Function

Based on the above network design, the overall loss function for training on synthetic datasets is:

$$\mathcal{L}_{\text{synthetic}} = \mathcal{L}_{\text{collaborative}} + \mathcal{L}_{\text{mscc}}. \quad (5)$$

Online-update Learning

Since a deraining model trained on synthetic data normally does not generalize well to real-world images, we propose an online-update learning approach to fine-tune the model on real-world rainy images. The key challenges are two-fold. The first is that there are no ground-truth images available for training. The second is how to keep the training stable and improve the model performance. To address these issues, we use the derained results of real-world images generated by the model trained on synthetic data as pseudo ground truth and update the pseudo ground truth at each epoch with the fine-tuned model. The loss function is based on Kullback-Leibler divergence and defined as:

$$\mathcal{L}_{\text{real}} = \underbrace{\|\hat{B}^k - \hat{B}^{k-1}\|_1}_{\text{content term}} + \underbrace{\lambda KL_{\text{Loss}}(\hat{R}^k, \hat{R}_{\text{random}}^{k-1})}_{\text{regularization term}}, \quad (6)$$

where \hat{B}^k and \hat{B}^{k-1} are the deraining results of a real-world rainy image O generated by the model \mathcal{B} at epoch k and $k-1$ respectively. Note that \hat{B}^0 is the initial deraining result produced by \mathcal{B} after training on synthetic data. $\hat{R}^k = O - \hat{B}^k$ is the estimated rain streaks of O . $\hat{R}_{\text{random}}^{k-1} = O_{\text{random}} - \hat{B}_{\text{random}}^{k-1}$

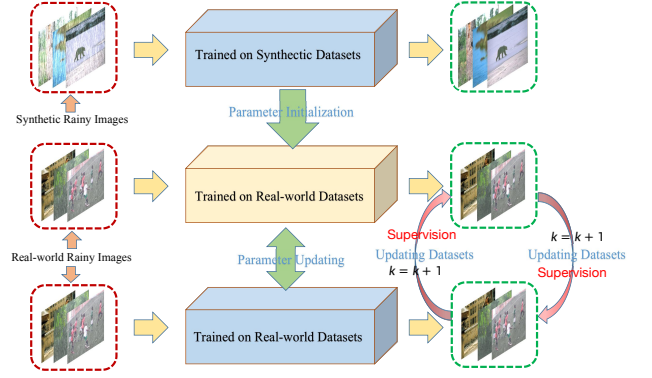


Figure 5: Proposed online-update learning approach.

Algorithm 1: Online-update Learning on Real-world Data

Preparation: The initial deraining result \hat{B}^0 of a real-world image O generated by the model trained on synthetic data.

Input: $\{O, \hat{B}^0\}$.

Output: Derained image $\{\hat{B}\}$.

- 1: While $k \leq \text{Epoch}_{\text{Real}}$ do:
- 2: Randomly crop training image pairs $\{O, \hat{B}^{k-1}\}$
- 3: Randomly select a real-world rainy image O_{random} and obtain $\hat{R}_{\text{random}}^{k-1} = O_{\text{random}} - \hat{B}_{\text{random}}^{k-1}$
- 4: Update the deraining model by Eq. (6)
- 5: Output the current deraining result: $\{\hat{B}^k\}$
- 6: Update the pseudo ground truth: $\{\hat{B}^{k-1}\} \leftarrow \{\hat{B}^k\}$
- 7: $k \leftarrow k + 1$
- 8: End while

is the estimated rain streaks of a randomly selected real-world rainy image O_{random} and $\hat{B}_{\text{random}}^{k-1}$ is the deraining result of O_{random} at epoch $k-1$. The first term of Eq. (6) ensures the content of image background consistent between different epochs and keeps the training stable, and the second term is a regularization term that enforces similarity in rain streaks and improves the deraining performance as the training proceeds (see Fig. 11). The fine-tuning process is illustrated in Fig. 5 and described in Alg. 1.

Experiments

We compare the proposed approach with 11 state-of-the-art methods (SOTAs), including RESCAN (Li et al. 2018b), NLEDN (Li et al. 2018a), SSIR (Wei et al. 2019), PreNet (Ren et al. 2019), SpaNet (Wang et al. 2019b), DCSFN (Wang et al. 2020b), MSPFN (Jiang et al. 2020), DRDNet (Deng et al. 2020), RCDNet (Wang et al. 2020c), Syn2Real (Yasarla, Sindagi, and Patel 2020), and MPRNet (Zamir et al. 2021), on five widely used synthetic datasets and a real-world dataset.

Datasets and Evaluation Criteria

Synthetic dataset We use Rain200H (Yang et al. 2017), Rain200L (Yang et al. 2017), Rain1200 (Zhang and Patel

Methods	Rain200H		Rain200L		Rain1200		Rain1400		Rain12		# Param
	PSNR \uparrow	SSIM \uparrow	PSNR \uparrow	SSIM \uparrow	PSNR \uparrow	SSIM \uparrow	PSNR \uparrow	SSIM \uparrow	PSNR \uparrow	SSIM \uparrow	
RESCAN (ECCV'18)	26.661	0.8419	36.993	0.9788	32.127	0.9028	30.969	0.9117	32.965	0.9545	0.15M
NLEDN (MM'18)	27.315	0.8904	36.487	0.9792	32.473	0.9198	31.014	0.9206	33.028	0.9615	1.01M
SSIR (CVPR'19)	14.420	0.4501	23.476	0.8026	24.427	0.7713	25.772	0.8224	24.138	0.7768	0.06M
PreNet (CVPR'19)	27.525	0.8663	34.266	0.9660	30.456	0.8702	30.984	0.9156	35.095	0.9400	0.17M
SpaNet (CVPR'19)	25.484	0.8584	36.075	0.9774	27.099	0.8082	29.000	0.8891	33.217	0.9546	0.28M
DCSFN (MM'20)	28.469	0.9016	37.847	0.9842	32.275	0.9228	31.493	0.9279	35.803	0.9683	6.45M
MSPFN (CVPR'20)	25.553	0.8039	30.367	0.9219	30.382	0.8860	31.514	0.9203	34.253	0.9469	21.00M
DRDNet (CVPR'20)	15.102	0.5028	37.465	0.9806	28.386	0.8574	28.359	0.8574	25.435	0.7550	5.23M
RCDNet (CVPR'20)	28.698	0.8904	38.400	0.9841	32.273	0.9111	31.016	0.9164	31.038	0.9069	3.67M
Syn2Real (CVPR'20)	14.495	0.4021	31.035	0.9365	28.812	0.8400	28.582	0.8586	31.038	0.9069	2.62M
MPRNet (CVPR'21)	29.949	0.9151	36.610	0.9785	33.655	0.9310	32.257	0.9325	36.578	0.9696	3.64M
Ours	29.985	0.9218	39.284	0.9875	33.718	0.9327	32.617	0.9334	36.851	0.9714	2.04M

Table 1: Quantitative results on five synthetic datasets. The best results are marked in **bold**. \uparrow denotes higher is better.



Figure 6: Comparison with state-of-the-art methods on synthetic datasets. The proposed network is able to restore better texture.

2018), Rain1400 (Fu et al. 2017), and Rain12 (Li et al. 2016) as the synthetic datasets for training and evaluation. Rain200H is the most challenging dataset, which has 1800 image pairs for training and 200 pairs for testing. Rain200L is the easiest dataset with the same number of training and testing samples as Rain200H. Rain1200 has images with heavy, middle, and light rain, and there are 4000 training images and 400 testing images for each density. Rain1400 has 12600 training samples and 1400 testing samples. Since Rain12 only contains 12 testing samples, we use the model trained on Rain200H to test the deraining results. We use Rain200H as the dataset for ablation study and analysis.

Real-world dataset Yang et al. (2017), Li et al. (2019), and Wang et al. (2020a) provide a large body of real-world rainy images. We use them to evaluate the deraining results on real-world data.

Evaluation criteria We use two widely used metrics, peak signal to noise ratio (PSNR) (Huynh-Thu and Ghanbari 2008) and structural similarity index measure (SSIM) (Wang et al. 2004) to evaluate the quality of restored images on synthetic datasets. As there are no ground-truth for real-world rainy images, we only compare the results visually.

Implementation Details

We set the number of channels of each convolutional layer except the last one as 20, and LeakyReLU with $\alpha = 0.2$ is used after each convolutional layer except for the last one. For the last layer, we use 3×3 convolution without any activation function in \mathcal{B} , \mathcal{M} , and \mathcal{T} . We randomly crop 128×128 image patches as input, and the batch size is set as 12. We use ADAM optimizer (Kingma and Ba 2015) to train the network. The initial learning rate is 0.0005, which will be divided by 10 at the 300-th and 400-th epochs, and the model training terminates after 500 epochs. We set $\lambda = 0.0001$,

$\alpha_1 = 1$, $\alpha_2 = 1$, $\alpha_3 = 1$, $\beta_1 = 0.05$, and $\beta_2 = 0.001$. We train the model for 30 epochs on the real-world dataset, i.e., $\text{Epoch}_{\text{Real}} = 30$. Our model is trained with four NVIDIA RTX TITAN GPUs on the Pytorch platform.

Results and Analysis on Synthetic Datasets

Comparisons with SOTAs on Synthetic Datasets Tab. 1 reports the results of our method and SOTAs on five synthetic datasets. We can see that our method achieves the best results on all tested datasets in PSNR and SSIM. We further show some deraining results in Fig. 6. It can be observed that our method can restore better details and textures and obtain clearer background images, while other approaches hand down some rain streaks or lose some details.

Analysis on BiSCSM We analyze the effect of different components of BiSCSM and report the results in Tab. 2. Note that the method (M_1) does not generate better results if we remove BiSCSM from the encoder-decoder framework. Furthermore, we replace the Down-to-Up and Up-to-Down operations in BiSCSM by element-wise summation (M_2) and 1×1 convolution (M_3) to fuse features at different scales. We find that both operations do not perform well compared to the proposed ones, demonstrating the effectiveness of the mining modules. Fig. 7 visualizes the feature maps before and after BiSCSM. One can see that the features are significantly enhanced after BiSCSM. We also test the single-directional mining modules, i.e., using Down-to-Up (M_4) or Up-to-Down (M_5) mining module alone, and the results show the bidirectional manner is better and can mine richer features for better deraining (M_4 and M_5 vs. M_7). Finally, we observe that position awareness can improve the deraining performance (M_6 vs. M_7).

Analysis on MSCC Compared with deep models that have no constraints on intermediate layers, our proposed

Experiments	M_1	M_2	M_3	M_4	M_5	M_6	M_7 (Ours)
Sum	✗	✓	✗	✗	✗	✗	✗
Conv $_{1\times 1}$	✗	✗	✓	✗	✗	✗	✗
Down-to-Up	✗	✗	✗	✓	✗	✗	✗
Up-to-Down	✗	✗	✗	✗	✓	✗	✗
BiSCSM	✗	✗	✗	✗	✗	✓	✓
Position	✗	✓	✓	✓	✓	✓	✓
PSNR \uparrow	29.583	29.625	29.541	29.393	29.828	29.953	29.985
SSIM \uparrow	0.9168	0.9177	0.9156	0.9172	0.9201	0.9218	0.9218

Table 2: Ablation study of BiSCSM. ✓ and ✗ denote that the corresponding component is adopted and not adopted, respectively.

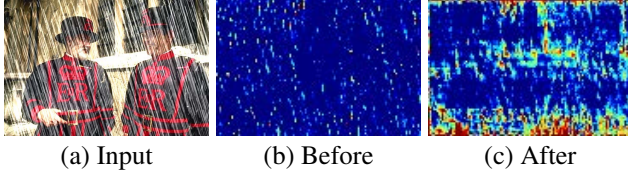


Figure 7: Visualization of the feature maps before and after BiSCSM.

Experiments	R_1	R_2	R_3	R_4	R_5 (Ours)
1/2 Scale	✗	✓	✗	✗	✓
1/4 Scale	✗	✗	✓	✗	✓
Full Scale	✗	✗	✗	✓	✗
PSNR \uparrow	29.824	29.879	29.839	29.970	29.985
SSIM \uparrow	0.9195	0.9209	0.9204	0.9211	0.9218

Table 3: Ablation study of the multi-scale compact constraints.

MSCC can make the deep network more compact and learn more useful features. Tab. 3 shows the results of different types of constraints. We observe that the model without any constraints (R_1) performs the worst, while the results get better as we add different constraints and reach the best when both 1/2 (R_2) and 1/4 (R_3) scale constraints are added.

We also consider replacing the 1/2 and 1/4 scale images with full-scale images to constrain the network. The comparison between R_4 and R_5 demonstrates that full-scale images are less effective than the multi-scale images, which is probably due to the better structures of Laplacian pyramid images.

Ablation Study on Collaborative Learning We conduct an ablation study of the proposed collaborative network in Tab. 4. The results show that the model achieves the best performance when the sub-networks \mathcal{T} and \mathcal{M} are learned with \mathcal{B} in a collaborative manner.

We also consider a case by cascading the three sub-networks to form a deep network model. Specifically, we cascade the network modules $\mathcal{N}_{11}, \mathcal{N}_{12}, \mathcal{N}_{13}, \mathcal{N}_{21}, \mathcal{N}_{22},$ and \mathcal{N}_{31} and ensure the cascaded network has roughly the same number of parameters as the collaborative network. We find that the cascaded network does not perform as well as the collaborative network, which further demonstrates the effectiveness of the proposed collaborative learning manner.

	w/o \mathcal{T} & w/o \mathcal{M}	w/o \mathcal{T} & w/ \mathcal{M}	Cascaded	w/ \mathcal{T} & w/ \mathcal{M} (Ours)
PSNR \uparrow	29.563	29.355	29.642	29.985
SSIM \uparrow	0.9158	0.9146	0.9188	0.9218

Table 4: Ablation study on collaborative learning.

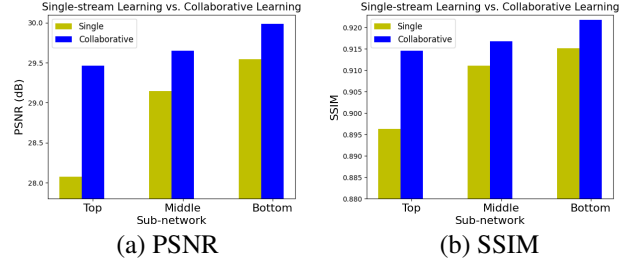


Figure 8: Comparison between single-stream learning and collaborative learning.

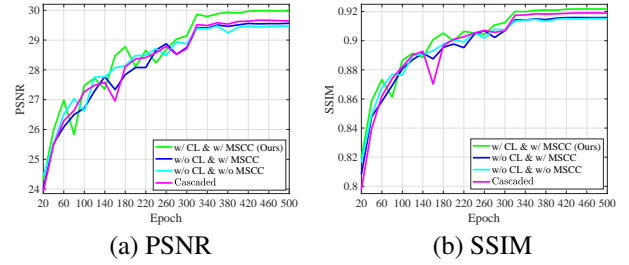


Figure 9: Further ablation study on collaborative learning (CL) and multi-scale compact constraints (MSCC).

Comparison between Single-stream Learning and Collaborative Learning In Fig. 8, we provide the comparison of the performance of each sub-network trained in single-stream learning and collaborative learning manners for image deraining. Single-stream learning means training the sub-networks \mathcal{T} , \mathcal{M} , and \mathcal{B} independently. The results show that the sub-networks trained by collaborative learning perform much better than by single-stream learning. It can be also observed that the sub-network \mathcal{T} trained by collaborative learning generates comparable results as the sub-network \mathcal{B} trained by single-stream learning, while the size of \mathcal{T} is two-thirds of \mathcal{B} .

Further Ablation Study on Collaborative Learning and Multi-scale Compact Constraints Fig. 9 provides a further ablation study of collaborative learning and multi-scale compact constraints, where the learning curves of different variants are plotted. The results show that both collaborative learning and multi-scale compact constraints are useful for improving the deraining performance. It can also be observed that without either collaborative learning or multi-scale compact constraints, the models perform worse than the cascaded network, which further demonstrates the effectiveness of the proposed external and internal learning manners for the deraining task.

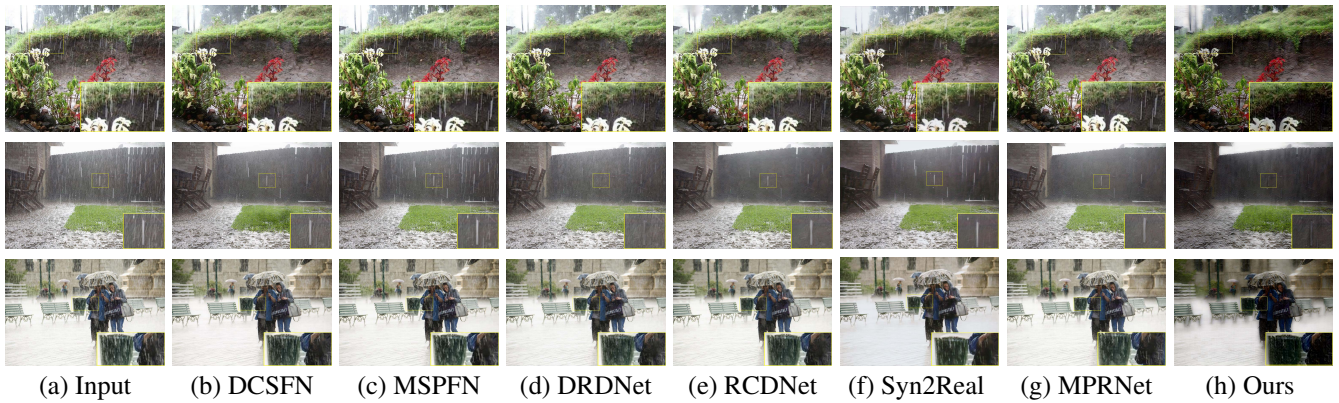


Figure 10: Comparisons with state-of-the-art methods on real-world images. Our proposed online-update learning approach is able to deal with various rainy conditions to better remove rain streaks and even haze and recover clearer images.



Figure 11: Ablation study of the proposed online-update learning approach. (a) Input. (b) Only trained on synthetic data. (c) Directly fine-tuned on real-world images. (d) Online-update learning on real-world images.



Figure 12: Applying the proposed online-update learning approach on DCSFN (Wang et al. 2020b). (a) Input. (b) Only trained on synthetic data. (c) Directly fine-tuned on real-world images. (d) Online-update learning on real-world images.

Results and Analysis on Real-world Datasets

Comparisons with SOTAs on Real-world Images We further demonstrate the effectiveness of our method on the real-world dataset by comparing with state-of-the-art methods. Fig. 10 presents the deraining results of several challenging cases. It can be observed that our method produces cleaner and clearer deraining results than others, demonstrating its effectiveness in removing rain streaks of real-world rainy images.

Effectiveness of the Online-update Learning Approach Fig. 11 presents the ablation study of the online-update learning manner. Compared with only using synthetic data to train the model (Fig. 11(b)) or directly fine-tuning the model on real-world images without updating the pseudo ground truth (Fig. 11(c)), our proposed online-update learning manner (Fig. 11(d)) is able to further improve the deraining performance on real-world images, demonstrating its effectiveness.

Generality of the Online-update Learning Approach To further demonstrate the effectiveness of the online-update learning approach for real-world image deraining, we apply it on a state-of-the-art method, DCSFN (Wang et al. 2020b). Similar to Fig. 11, Fig. 12 presents the results on a real-world rainy image by different ways of learning. It can be seen that the proposed online-update learning approach can be successfully applied to DCSFN to significantly improve its deraining performance on real-world images. Since the

online-update learning approach is generic, we believe it be applied to many other existing methods to improve their performance in real-world image deraining.

Conclusion

In this paper, we have proposed a high-order collaborative network with multi-scale compact constraints to control the learning process in an external and internal manner for image deraining. We have further developed a bidirectional scale-content similarity mining module to learn useful features at different scales in a down-to-up and up-to-down way to facilitate rain streaks removal. Finally, to improve the deraining performance on real-world images, we have proposed an effective online-update learning approach to fine-tune the deraining model on real-world rainy images in a self-supervised manner. Extensive experiments show that the proposed model outperforms state-of-the-art methods on five public synthetic datasets and one real-world dataset.

Acknowledgements

We would like to thank the anonymous reviewers for their helpful comments. This work was supported by the Fundamental Research Funds for the Central Universities (No. 30920041109), and the Grant of DaSAIL Project P0030935 funded by PolyU/UGC.

References

- Chen, Y.; and Hsu, C. 2013. A Generalized Low-Rank Appearance Model for Spatio-temporally Correlated Rain Streaks. In *IEEE ICCV*, 1968–1975.
- Deng, S.; Wei, M.; Wang, J.; Feng, Y.; Liang, L.; Xie, H.; Wang, F. L.; and Wang, M. 2020. Detail-recovery Image Deraining via Context Aggregation Networks. In *IEEE CVPR*, 14548–14557.
- Fu, X.; Huang, J.; Zeng, D.; Huang, Y.; Ding, X.; and Paisley, J. 2017. Removing Rain from Single Images via a Deep Detail Network. In *IEEE CVPR*, 1715–1723.
- Hu, X.; Fu, C.; Zhu, L.; and Heng, P. 2019. Depth-Attentional Features for Single-Image Rain Removal. In *IEEE CVPR*, 8022–8031.
- Huynh-Thu, Q.; and Ghanbari, M. 2008. Scope of validity of PSNR in image/video quality assessment. *Electronics Letters*, 44(13): 800–801.
- Jiang, K.; Wang, Z.; Yi, P.; Chen, C.; Huang, B.; Luo, Y.; Ma, J.; and Jiang, J. 2020. Multi-Scale Progressive Fusion Network for Single Image Deraining. In *IEEE CVPR*, 8343–8352.
- Kang, L.; Lin, C.; and Fu, Y. 2012. Automatic Single-Image-Based Rain Streaks Removal via Image Decomposition. *IEEE TIP*, 21(4): 1742–1755.
- Kingma, D. P.; and Ba, J. 2015. Adam: A Method for Stochastic Optimization. In *ICLR*.
- Li, G.; He, X.; Zhang, W.; Chang, H.; Dong, L.; and Lin, L. 2018a. Non-locally Enhanced Encoder-Decoder Network for Single Image De-raining. In *ACM MM*, 1056–1064.
- Li, S.; Araujo, I. B.; Ren, W.; Wang, Z.; Tokuda, E. K.; Junior, R. H.; Cesar-Junior, R.; Zhang, J.; Guo, X.; and Cao, X. 2019. Single Image Deraining: A Comprehensive Benchmark Analysis. In *IEEE CVPR*, 3838–3847.
- Li, X.; Wu, J.; Lin, Z.; Liu, H.; and Zha, H. 2018b. Recurrent Squeeze-and-Excitation Context Aggregation Net for Single Image Deraining. In *ECCV*, 262–277.
- Li, Y.; Tan, R. T.; Guo, X.; Lu, J.; and Brown, M. S. 2016. Rain Streak Removal Using Layer Priors. In *IEEE CVPR*, 2736–2744.
- Luo, Y.; Xu, Y.; and Ji, H. 2015. Removing Rain from a Single Image via Discriminative Sparse Coding. In *IEEE ICCV*, 3397–3405.
- Mei, Y.; Fan, Y.; Zhang, Y.; Yu, J.; Zhou, Y.; Liu, D.; Fu, Y.; Huang, T. S.; and Shi, H. 2020a. Pyramid Attention Networks for Image Restoration. *arXiv preprint arXiv:2004.13824*.
- Mei, Y.; Fan, Y.; Zhou, Y.; Huang, L.; Huang, T. S.; and Shi, H. 2020b. Image Super-Resolution With Cross-Scale Non-Local Attention and Exhaustive Self-Exemplars Mining. In *IEEE CVPR*, 5689–5698.
- Mei, Y.; Fan, Y.; Zhou, Y.; Huang, L.; Huang, T. S.; and Shi, H. 2020c. Image Super-Resolution With Cross-Scale Non-Local Attention and Exhaustive Self-Exemplars Mining. In *IEEE CVPR*, 5689–5698.
- Pan, J.; Dong, J.; Liu, Y.; Zhang, J.; Ren, J. S. J.; Tang, J.; Tai, Y.; and Yang, M. 2021. Physics-Based Generative Adversarial Models for Image Restoration and Beyond. *IEEE TPAMI*, 43(7): 2449–2462.
- Pan, J.; Liu, S.; Sun, D.; Zhang, J.; Liu, Y.; Ren, J. S. J.; Li, Z.; Tang, J.; Lu, H.; Tai, Y.; and Yang, M. 2018. Learning Dual Convolutional Neural Networks for Low-Level Vision. In *IEEE CVPR*, 3070–3079.
- Ren, D.; Zuo, W.; Hu, Q.; Zhu, P.; and Meng, D. 2019. Progressive Image Deraining Networks: A Better and Simpler Baseline. In *IEEE CVPR*, 3937–3946.
- Wang, C.; Wu, Y.; Su, Z.; and Chen, J. 2020a. Joint Self-Attention and Scale-Aggregation for Self-Calibrated Deraining Network. In *ACM MM*, 2517–2525.
- Wang, C.; Xing, X.; Wu, Y.; Su, Z.; and Chen, J. 2020b. DCSFN: Deep Cross-scale Fusion Network for Single Image Rain Removal. In *ACM MM*, 1643–1651.
- Wang, C.; Zhang, M.; Su, Z.; Wu, Y.; Yao, G.; and Wang, H. 2019a. Learning a multi-level guided residual network for single image deraining. *Signal Process. Image Commun.*, 78: 206–215.
- Wang, H.; Xie, Q.; Zhao, Q.; and Meng, D. 2020c. A Model-Driven Deep Neural Network for Single Image Rain Removal. In *IEEE CVPR*, 3100–3109.
- Wang, T.; Yang, X.; Xu, K.; Chen, S.; Zhang, Q.; and Lau, R. W. H. 2019b. Spatial Attentive Single-Image Deraining With a High Quality Real Rain Dataset. In *IEEE CVPR*, 12270–12279.
- Wang, Z.; Bovik, A. C.; Sheikh, H. R.; and Simoncelli, E. P. 2004. Image quality assessment: from error visibility to structural similarity. *IEEE TIP*, 13(4): 600–612.
- Wang, Z.; Wang, C.; Su, Z.; and Chen, J. 2021. Dense Feature Pyramid Grids Network for Single Image Deraining. In *IEEE ICASSP*, 2025–2029.
- Wei, W.; Meng, D.; Zhao, Q.; Xu, Z.; and Wu, Y. 2019. Semi-Supervised Transfer Learning for Image Rain Removal. In *IEEE CVPR*, 3877–3886.
- Yang, W.; Tan, R. T.; Feng, J.; Liu, J.; Guo, Z.; and Yan, S. 2017. Deep Joint Rain Detection and Removal from a Single Image. In *IEEE CVPR*, 1685–1694.
- Yasarla, R.; Sindagi, V. A.; and Patel, V. M. 2020. Syn2Real Transfer Learning for Image Deraining Using Gaussian Processes. In *IEEE CVPR*, 2723–2733.
- Zamir, S. W.; Arora, A.; Khan, S.; Hayat, M.; Khan, F. S.; Yang, M.; and Shao, L. 2021. Multi-Stage Progressive Image Restoration. In *IEEE CVPR*.
- Zhang, H.; and Patel, V. M. 2017. Convolutional Sparse and Low-Rank Coding-Based Rain Streak Removal. In *IEEE WACV*, 1259–1267.
- Zhang, H.; and Patel, V. M. 2018. Density-Aware Single Image De-Raining Using a Multi-Stream Dense Network. In *IEEE CVPR*, 695–704.
- Zhu, H.; Wang, C.; Zhang, Y.; Su, Z.; and Zhao, G. 2020. Physical Model Guided Deep Image Deraining. In *IEEE ICME*, 1–6.